Hindawi
Geofluids
Volume 2021, Article ID 4348912, 13 pages
https://doi.org/10.1155/2021/4348912

Research Article

Crack Propagation Law and Failure Characteristics of Coal-Rock Combined Body with the Different Inclination Angle of Prefabricated Fissure

Chunlei Zhang,[1] **Yun Dong**,[1] **Ruimin Feng**,[2] **Ningbo Peng**,[1] **Jihua Zhang**,[1] **Jingke Wu**,[1] **and Wei Shen**[1]

[1]*Faculty of Architecture and Civil Engineering, Huaiyin Institute of Technology, Huai'an, Jiangsu 223001, China*
[2]*Department of Civil Engineering, University of Arkansas, 4190 Bell Engineering Center, Fayetteville, AR 72701, USA*

Correspondence should be addressed to Chunlei Zhang; leizhewudi@hyit.edu.cn and Yun Dong; dyunhyit@hyit.edu.cn

Received 26 April 2021; Accepted 18 June 2021; Published 5 July 2021

Academic Editor: Feng Du

Few studies have been conducted on the crack propagation law and failure characteristics of coal-rock combined body (CRCB) with prefabricated fissure. A sliding crack model was firstly presented to analyze the failure law of rock with a single fracture and the influence of the inclination angle of the fracture on the strength of the rock. The RFPA numerical models of the CRCB with different inclination angles of prefabricated fracture were then established to simulate the dynamic change process of crack propagation and shear stress of the CRCB with prefabricated fracture under uniaxial compression. The influence of the inclination angle of the fracture in the rock on the fracture expansion and failure characteristics of CRCB was further analyzed based on the acoustic emission data. The results showed that (1) when $2\beta = \arctan 1/\mu$, σ_{cw} takes the minimum value, and crack initiation is most likely to occur; (2) the strength of coal-rock assemblage shows different changing trends with the fracture inclination angle; (3) the secondary cracks of CRCB with prefabricated fracture of 0°, 15°, and 30° initiated and expanded near the tip of the main crack, and the secondary cracks of 45°, 60°, and 75° initiated and expanded from the tip of the main crack; (4) there are three failure modes of CRCB with prefabricated crack, the double-shear failure mode Λ, the tensile-shear composite failure mode along the fracture surface, and the tensile failure mode along the fracture surface; and (5) intact CRCB and CRCB with prefabricated crack when $\alpha = 75°$ and $\alpha = 90°$ have strong brittleness, and other CRCB with different prefabricated fracture inclination angles show a certain degree of postpeak plasticity. The results on the mechanical properties and damage characteristics of CRCB are of great significance for the safety and efficient mining of deep coal resources.

1. Introduction

Coal is the main resource of energy supply in China. As coal in the shallow subsurface is gradually exhausted, coal mining depth is constantly increasing, which leads to the frequent occurrence of dynamic disasters such as coal and gas outburst and rock burst under deep high geostress environment [1, 2]. The deformation damage of coal-rock combined body (CRCB) in the deep environment is affected by multiple factors such as its own physical and mechanical properties and geological structure, but more importantly, it is affected by the coexistence of the coal-rock combination structure [3]. The damage and break of rock mass and coal in the engineering scale are tightly associated with their fine structural features. Research in microscopic view provides a powerful tool to better understand and master the damage and breakage of coal and rock mass in the engineering scale [4]. A better understanding of damage characteristics and fracture mechanisms of CRCB is much helpful for us to make a reasonable interpretation on mining-induced breakage, fracture development, and stress change in the field. Therefore, research on the mechanical properties and damage characteristics of CRCB is of great significance for the safety and efficient mining of deep coal resources.

In recent years, many scholars have carried out mechanical tests of CRCB under different conditions either by

numerical simulations or laboratory tests, aiming to explore the mechanical response characteristics of CRCB [5]. Gong et al. [6, 7] obtained outburst proneness of different CRCB using the axial loading test based on prepeak energy distribution and different loading rates. Zuo et al. [8, 9] studied the failure modes and mechanical behavior differences of different CRCB under uniaxial and triaxial compression. Cao et al. [10] considered the influence of the interface inclination angle of CRCB on its strength and failure mechanism. Liu et al. and Xie et al. [11, 12] studied the crack propagation law of CRCB with different combinations and found that the failure of coal and the propagation of cracks further led to the failure of the rock. Du and Wang [13] explored the failure characteristics of CRCB through the true triaxial test. Chen et al., Zhao et al., and Dong et al. [14–16] obtained the fracture propagation mode of CRCB under different loading conditions through theoretical analysis and laboratory experiments. The above research on the failure characteristics of CRCB is mainly aimed at intact coal-rock assemblages. However, considering the influence of geological movement during the formation of coal and rock masses, there are a large number of original fissures in the coal and rock masses which affect the "coal-rock" structural strength and failure characteristics, so it is worth investigating the role of the fissures in the mechanical behavior of the rocks. Li et al. and Yin et al. [17–19] used Split Hopkinson Pressure Bar (SHPB) and PFC numerical simulation methods to perform shock compression and uniaxial compression tests on CRCB with prefabricated cracks and obtained the crack inclination and position on the influence of the strength and failure characteristics of the CRCB, but the influence of the cracks in the rock mass is not considered.

Therefore, this paper will use RFPA software to carry out numerical simulations of CRCB with prefabricated cracks in different inclination angles, explore the influence of cracks in rock mass on the mechanical properties and failure characteristics of the CRCB, and further explore the mechanical response characteristics of the CRCB.

2. Sliding Crack Model of Rock with Single Fracture

At present, there are two main views on the compression-induced crack propagation of brittle materials: one is compression-tension fracture and the other is sliding fracture. Comparing the two views in explaining the microcrack propagation of brittle materials, the sliding crack model reflecting the mechanism of microcrack sliding opening fracture gradually prevails and has been widely accepted in academia. Natural rock material has the characteristics of discontinuity, inelasticity, heterogeneity, and anisotropy. Its structural composition is relatively complex, and it belongs to the brittle material. In 1963, Brace and Bombolakis [20] first proposed the sliding crack model, which was later popularized and applied to the study of the mechanical mechanism of fractured brittle materials under compressive loading by Horii and Nemat-Nasser [21].

2.1. Sliding Crack Model. The frictional sliding crack model is the most extensive model for studying coal and rock mass damage [22]. It is believed that when coal and rock mass is compressed, original cracks will produce secondary tensile cracks that propagate in the direction of maximum principal stress, and secondary cracks are the main cause of splitting and destruction of coal and rock mass. The friction crack model under compressive stress is shown in Figure 1.

The following assumptions are made for the model in Figure 1. The problem is a plane strain problem, the confining pressure is σ_3, and the axial pressure is σ_1, and the following assumptions are satisfied: The rock mass is homogeneous and isotropic; both the rock strength and fracture strength obey the Mohr-Coulomb strength criterion. The angle between the penetration crack and the axial stress is β, the internal friction angle is φ_w, the cohesion of the fracture surface is cw, the normal stress vertical to fracture surface is σ, and the shear stress along the fracture surface is τ.

Decompose the shear stress and normal stress on the original crack surface PP_1 to get

$$\begin{cases} \sigma_n = \sigma_1 \cos^2\theta + \sigma_3 \sin^2\theta, \\ \tau_e = \dfrac{1}{2}(\sigma_1 - \sigma_3) \sin 2\theta. \end{cases} \tag{1}$$

It is assumed that the failure of coal and rock mass satisfies the Mohr-Coulomb criterion. The actual effective shear stress of friction sliding can be then expressed as

$$\tau_{\text{eff}} = (\sigma_1 - \sigma_2) \cos\theta \sin\theta - \tau_c - \mu\left(\sigma_1 \cos^2\theta + \sigma_2 \sin^2\theta\right), \tag{2}$$

where u is the internal friction coefficient of coal and rock mass and τ_c is the cohesion. The critical condition for frictional sliding of cracks is $\tau_{\text{eff}} = 0$, and we have

$$\sigma_1 = \frac{\sigma_2 \sin\theta \cos\theta - \tau_c - \mu\sigma_2 \cos^2\theta}{\mu \sin^2\theta + \sin\theta \cos\theta}. \tag{3}$$

According to the above equation, when $\theta_0 = \tan^{-1}(\mu + \sqrt{\mu^2 + 1})$, σ_1 gets the minimum value; then, we obtain the critical stress condition causing frictional sliding:

$$\sigma_{1cs} = \frac{\sigma_2 \sin\theta_0 \cos\theta_0 - \tau_c - \mu\sigma_2 \cos^2\theta_0}{\mu \sin^2\theta_0 + \sin\theta_0 \cos\theta_0}. \tag{4}$$

When $\sigma_1 < \sigma_{1cs}$, the coal and rock mass materials exhibit elastic characteristics, and the original cracks do not cause friction sliding. When $\sigma_{1cs} \le \sigma_1 < \sigma_{1c}$, the coal and rock mass exhibits nonlinear strengthening characteristics, and some cracks have self-similar propagation and frictional sliding.

Continuing to load, some cracks will self-similarly propagate. The crack gradually expands to a certain characteristic length c_b with the increase of axial pressure, and c_b is related to the material composition of coal and rock mass.

In the rock loading test, the cracks of the rock sample experience a process from opening to closing to expansion

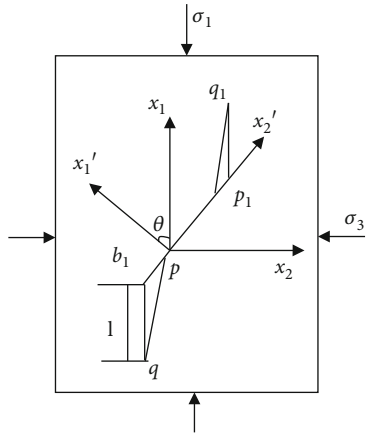

Figure 1: Frictional sliding crack model under compressive loading (the overall coordinate system o-x_1x_2 and the local coordinate system o-$x_1'x_2'$; the ox_1' axis is parallel to the crack's outer normal line; the length of the crack is 2c, and the azimuth angle is θ).

and rupture. Therefore, to study the influence of cracks on the strength of the rock in the compression test, it is necessary to start with the closed crack [23]. Because the crack is closed, the effective shear stress on the crack causes relative sliding on the crack surface, which can be regarded as a pure type II crack at the crack initiation stage, that is, KI = 0 [24]; according to the theory of fracture mechanics, the stress intensity factor at the crack tip is

$$k_{\mathrm{II}} = \tau_e \sqrt{\pi c}. \tag{5}$$

Taking $\sigma_3 = 0$ and $\sigma = \sigma_1$ and substituting Equation (2) into Equation (5), we have

$$k_{\mathrm{II}} = \tau_e \sqrt{\pi c} = \sigma \cos\theta \sin\theta \sqrt{\pi c} - \tau_c \sqrt{\pi c} - \mu\sigma \cos^2\theta \sqrt{\pi c}. \tag{6}$$

For shear fracture under compression, the following formula is adopted as the criterion:

$$\lambda_{12} k_{\mathrm{I}} + k_{\mathrm{II}} = k_{\mathrm{IIc}}. \tag{7}$$

In the formula, λ_{12} is the compression reduction coefficient, and k_{IIc} is the shear toughness under compression. Since $k_{\mathrm{I}} = 0$, the failure criterion of the crack surface is $k_{\mathrm{II}} = k_{\mathrm{IIc}}$.

The criterion of stable growth of microcracks can be expressed as

$$K_{\mathrm{IIC}} = \frac{1}{2}\left[(\sin 2\theta - \mu - \mu \cos 2\theta)\sigma - 2\tau_c\right]\sqrt{\pi c}, \tag{8}$$

where a is the type II fracture toughness of the weak surface.

Since the cohesion τ_c of the crack surface during uniaxial compression is very small, take $\tau_c = 0$ and $\beta = 90°$-θ, the initial fracture strength of the crack is

$$\sigma_{cw} = \frac{2K_{\mathrm{IIC}}}{\sqrt{\pi c}(\sin 2\theta - \mu - \mu \cos 2\theta)} = \frac{2K_{\mathrm{IIC}}}{\sqrt{\pi c}(\sin 2\beta - \mu + \mu \cos 2\beta)}. \tag{9}$$

2.2. The Influence of Fissure Angle on the Strength of Rock Mass. No unified standard has been reported for the testing of type II fracture factor k_{IIc}; however, when the test model size, material, and the external conditions are all the same, the value of fracture toughness k_{IIc} only varies in a very small range if using the same loading method, and it can be considered that it remains unchanged during the experiment [25]. Under uniaxial compression, the strength and failure mode of a rock mass with a single closed crack are determined by the strength of the rock and the strength of the crack surface. It can be seen from Equation (9) that σ_{cw} is a function of β, c, and μ. When the crack length c and the friction coefficient μ of the crack surface is fixed, σ_{cw} is only related to the crack inclination angle. $\beta < \pi/2$-ψw is the discontinuity point of the function σ_{cw}. When $\beta > \pi/2$-ψw, $\sigma_{\mathrm{cw}} < 0$. At this time, the failure of the rock mass is due to tensile stress, which does not conform to the assumption. In order to obtain the extreme value of σ_{cw}, we take the derivative of Equation (9):

$$\frac{\partial \sigma_{\mathrm{cw}}}{\partial \beta} = 0, \quad \frac{\partial^2 \sigma_{\mathrm{cw}}}{\partial \beta^2} > 0. \tag{10}$$

It can be seen from Equation (10) that when $\beta = 1/2$ arctan $1/\mu$, Equation (10) holds. When $\beta = 1/2$ arctan $1/\mu$, σ_{cw} takes the minimum value, crack initiation is most likely to occur, and the corresponding crack initiation stress is the smallest. When μ is 0.1, $\beta = 42.145°$ [25].

3. Numerical Simulation

The RFPA (rock failure process analysis) software is adopted to study on the crack propagation law and failure characteristics of CRCB with prefabricated fissure. RFPA2D is a rock failure process analysis system with elastic mechanics as stress analysis tools, elastic damage theory, and modified Coulomb failure criterion as medium deformation and failure analysis module [26, 27], enabling to simulate the microcracking process of rock during the deformation process.

3.1. Model Construction and Parameter Selection. Figure 2 shows the model established for numerical simulation. The sample model is a rectangular CRCB with 100 mm height and 50 mm width. Both the height of coal and the height of rock in the model are 50 mm, and the model is divided into 200,000 units. Mohr-Coulomb is used as the constitutive relationship. The length of the crack is $20\sqrt{2}$ mm, and the closing cracks are in contact with each other, the crack surface friction coefficient is 0.1, and the fracture is located in rock, and the angles with the minimum principal stress are 0°, 15°, 30°, 45°, 60°, 75°, and 90°, respectively. Mechanical parameters of CRCB with prefabricated fissure are shown in Table 1. The uniaxial compression test was performed on the CRCB. The loading method was axial displacement

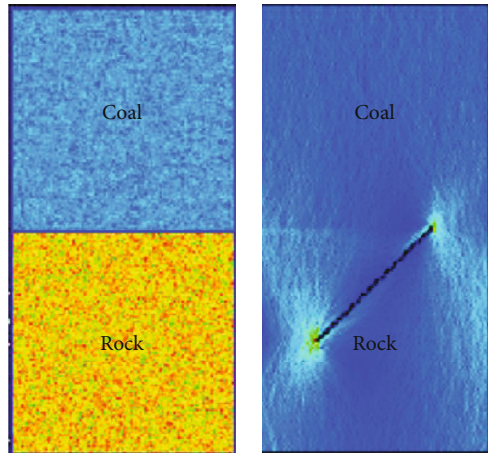

(a) Containing no crack (b) Containing 45° crack

Figure 2: Numerical models.

Table 1: Mechanical parameters of CRCB with prefabricated fissure.

Type	σ (MPa)	E (GPa)	ψ (°)	μ	ρ (kg·m^{-3})	m
Coal	50	12	32	0.25	1800	5
Rock	140	50	38	0.2	3500	10

loading with a one-step increment of 0.002 mm/step, and the load was carried out until the sample failed.

3.2. Analysis of Strength and Deformation Characteristics. The crack initiation stress σ_{ci} and the damage stress σ_{cd} are not only important characteristic values of CRCB strength but also the boundary point of different stages in the crack propagation process. There are many methods to determine the rock initiation stress and damage stress [28, 29]; in this paper, the axial stress corresponding to the crack initiation point is taken as the crack initiation stress σ_{ci}, and the damage stress σ_{cd} is determined by the axial stress corresponding to the rapid growth point of the crack. According to the fracture process of the CRCB (Figure 2), Table 2 shows the σ_{ci} and σ_{cd} of intact CRCB and CRCB with prefabricated fissure and their relationship with the uniaxial compressive strength σ of intact CRCB.

Figure 3 shows the fracture evolution process of CRCB with prefabricated fracture of different inclination angles (Due to space limitation, only the shear stress diagrams when the inclination angles of the fractures are $\alpha = 15°$ and $\alpha = 45°$ are listed). The generation, propagation, and penetration of microcracks formed the macroscopic failure surface of the CRCB, which in turn caused its failure and instability. As the axial strain increases, the evolution of the number of microcracks in CRCB with different inclination angles of crack is basically the same. There is initially no microcracks; microcracks slowly grow, then grow rapidly, and finally stabilize. The number of cracks increases sharply near the peak strain area, especially in a certain stage after the peak strain, which indicates that the microcracks within this stage are rapidly generated (step 26-2 of Figure 3(a) and step 27-4 of Figure 3(b)), expanded, and penetrated, forming macrocracks. The crack propagation and failure mode in intact CRCB and CRCB with prefabricated fracture of 90° are almost the same. The cracks have almost no effects on the crack propagation mode of the CRCB under uniaxial compression. The cracks start and propagate in the coal part, and no cracks show up in the rock part. The secondary cracks of CRCB with prefabricated fracture of 0°, 15°, and 30° initiated and expanded near the tip of the main crack, and the secondary cracks of 45°, 60°, and 75° initiated and expanded from the tip of the main crack. It can be seen from Figure 3 that the failure of the CRCB with $\alpha = 15°$ and $\alpha = 45°$ all experienced crack initiation, propagation, and final macroscopic failure, and the CRCB slipped along the crack surface during the failure process. The difference is that when $\alpha = 15°$, the initiation and propagation of secondary cracks do not appear at the tip of the main crack, but near the tip of the main crack. The crack propagation is relatively easy before the stress reaches the peak value, but the crack initiation stress is large. When step = 17, the crack initiation occurs, and the CRCB sample reaches its peak strength at step 39. When $\alpha = 45°$, the initiation and propagation of secondary cracks mainly spread around the tip of the main crack. As the loading continues, the stress intensity factor of the crack tip increases, and the microcracks penetrate through the tip of the main crack and at both ends of the main crack. Wing cracks are formed and propagate toward the crack end along the main loading direction. In addition, when $\alpha = 45°$, the crack initiation is much easier; when step = 10, the cracks start to initiate, and CRCB has been completely broken when the load reaches 29 steps, which is much easier to break compared with $\alpha = 15°$. Compared with $\alpha = 45°$, when $\alpha = 75°$, the crack angle is close to parallel to the axial loading direction, crack initiation is also easy, but the crack growth is strongly suppressed, which leads to an increase in its peak strength (Figure 4).

Figure 4 shows the stress-strain curves of CRCB with different prefabricated crack inclination angles. It can be seen that the CRCB with prefabricated fissure went through three

Table 2: Peak strength and peak strain of prefabricated fractured rock-coal combined body.

Angle (°)	σ_{ci}	Step	σ_{cd}	Step	Peak strength (σ) (MPa)	Peak strain (%)	Step	σ_{ci}/σ	σ_{cd}/σ
Intact	14.1	46	16.7	55	17.3	0.11	57	0.815	0.965
0	3.95	16	6.39	35	6.58	0.068	36	0.600	0.971
15	4.03	17	4.87	26	5.16	0.05	27	0.781	0.944
30	3.18	14	5.24	24	5.93	0.05	27	0.536	0.884
45	2.95	13	4.36	19	6.38	0.054	29	0.462	0.683
60	5.87	22	9.03	33	10.8	0.084	44	0.592	0.836
75	8.18	27	13.4	45	16.2	0.106	55	0.504	0.827
90	12.1	40	16.1	53	16.9	0.108	56	0.715	0.953

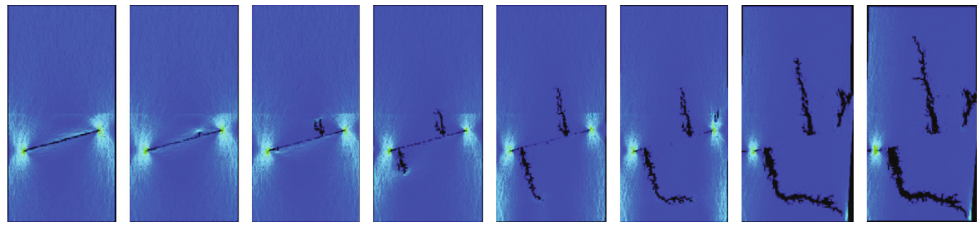

(a) When the prefabricated crack angle is 15° ($\alpha = 15°$)

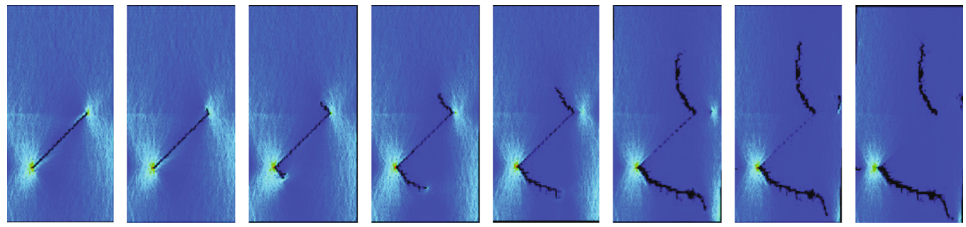

(b) When the prefabricated crack angle is 45° ($\alpha = 15°$)

Figure 3: Shear stress evolution processes for different prefabricated crack angles of CRCB.

stages under uniaxial compression: linear elastic deformation stage, fracture development stage, and failure stage. Different from the real rock test, the initial compaction stage does not show up obviously, which is mainly related to the constitutive model setting of the simulation software. The stress-strain curve basically rises linearly at the beginning of loading. When the stress reaches the peak strength, the CRCB begins to break, and meanwhile, the stress begins to drop. In addition, the peak strengths of CRCB with different fracture angles are different. Figure 5 shows the relationship between the peak strength of the CRCB and the inclination angle of the crack. It can be seen that the crack inclination angle affects the strength of the CRCB under uniaxial compression. As the crack inclination angle increases, the strength of the CRCB firstly decreases and then increases. CRCB has the lowest peak strength when $\alpha = 15°$. When $\alpha < 15°$, the peak strength of the CRCB decreases with the increase of the crack inclination angle. When $\alpha > 15°$, the peak strength of the CRCB increases with the increase of the inclination angle of the prefabricated fissure.

Compared with the intact CRCB, the bearing capacity of the CRCB with prefabricated fracture is reduced to a certain extent, that is, deterioration. In order to quantitatively express the degradation characteristics, the deterioration factor w is introduced and is expressed as

$$\omega = \left(1 - \frac{\sigma_0}{\sigma_\omega}\right) \times 100\%. \tag{11}$$

In the formula, σ_0 is the uniaxial compressive strength of the CRCB with prefabricated fissure (MPa) and σ_w is the uniaxial compressive strength of the CRCB with different prefabricated crack inclination angles (MPa).

Figure 6 shows the relationship between the deterioration factor and the crack inclination angle of the CRCB. As the inclination angle increases, the deterioration factor firstly increases and then decreases and reaches the maximum value when $\alpha = 15°$; as the inclination angle continues to increase, the deterioration factor decreases continuously until $\alpha = 75°$. When $\alpha = 90°$, the deterioration factor further decreases, which is close to the intact CRCB.

3.3. Failure Characteristic Analysis. Failure of the CRCB is caused by macroscopic cracks formed by the propagation of the prefabricated cracks in the rock and interpenetrating with each other, which in turn leads to the overall failure of the

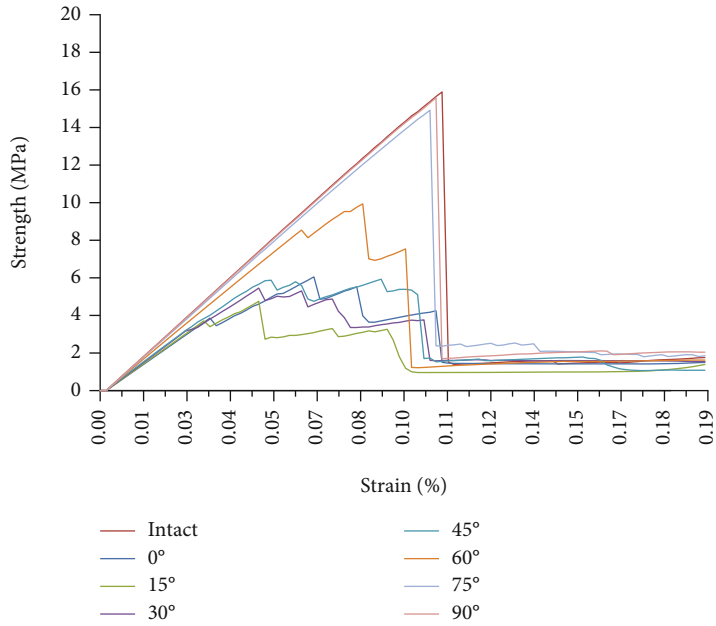

Figure 4: Stress-strain curves of coal-rock combined bodies.

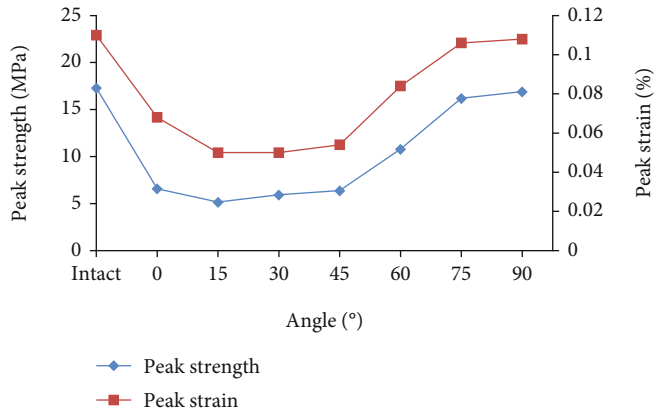

Figure 5: Curves of peak strength and peak strain of coal-rock combined body with prefabricated fissure.

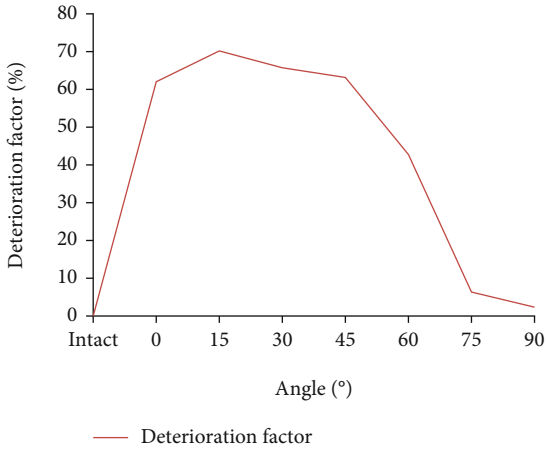

Figure 6: Deterioration factor curve.

CRCB. Therefore, the destruction of the rock mass in CRCB leads to its failure, and the inclination angle of the prefabricated cracks in the rock mass affects its failure mode. As shown in Figure 7, there are three failure modes of CRCB with prefabricated crack, the double-shear failure mode Λ (Figures 7(a), 7(g), and 7(h)), the tensile-shear composite failure mode along the fracture surface (Figures 7(b)–7(d)), and the tensile failure mode along the fracture surface (Figures 7(e) and 7(f)). The failure of the intact CRCB and the CRCB with 90° prefabricated fissures mainly occurs in the coal. This is mainly due to the fact that the strength of the coal sample is much smaller than that of the rock sample, and it is a double-shear failure mode, and the crack propagation is type Λ; the angle between the shear failure surface and the vertical direction is 47.3° and 33.8°, respectively; when the prefabricated fracture is 75° ($\alpha = 75°$), the CRCB also exhibits Λ-type double-shear failure, the difference is that the fracture expansion angle is reduced to 34.2° and 32°, and the crack tip

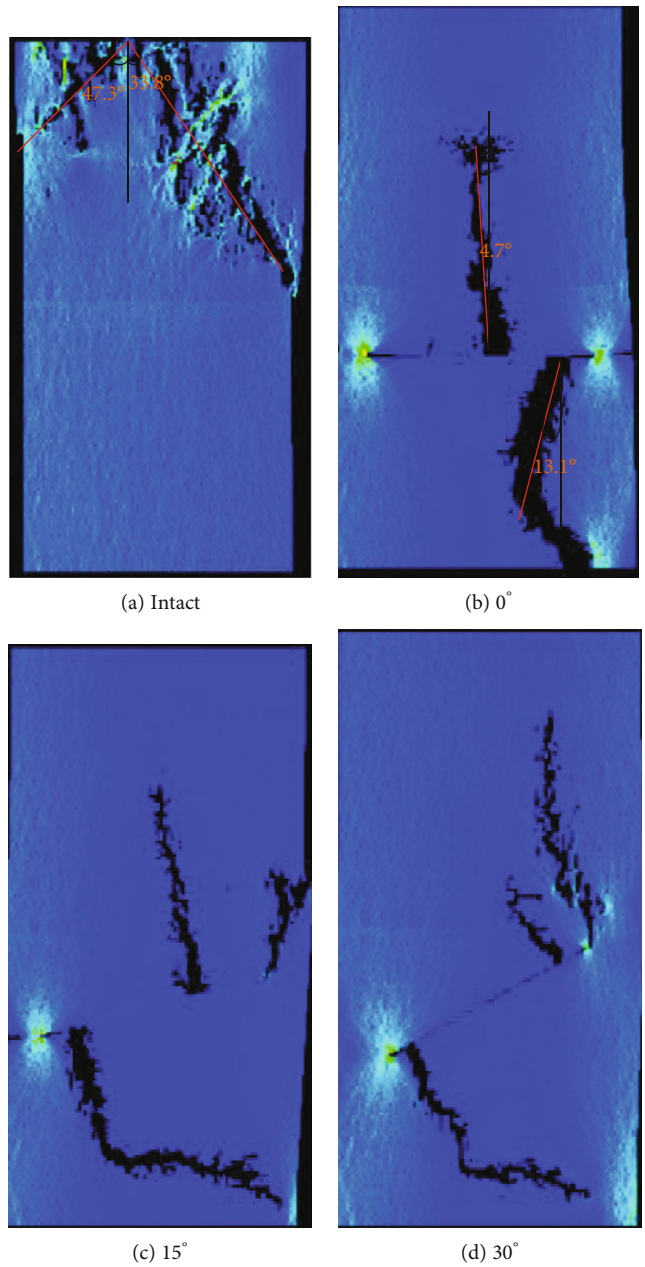

(a) Intact (b) 0°

(c) 15° (d) 30°

Figure 7: Continued.

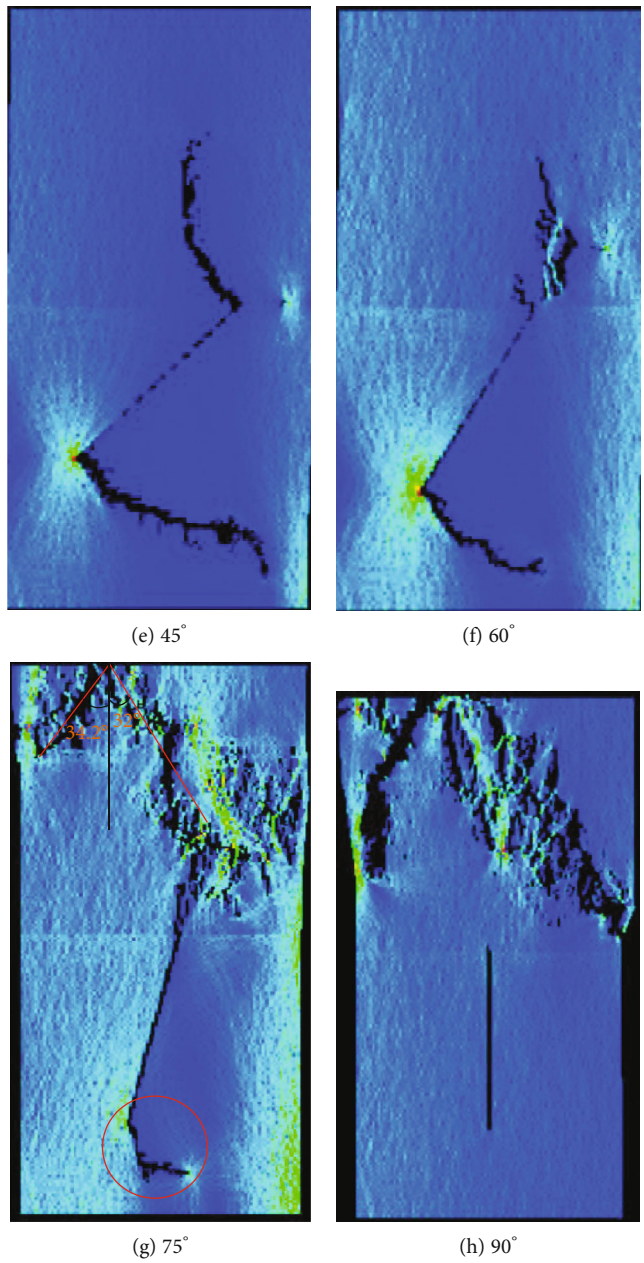

(e) 45° (f) 60°

(g) 75° (h) 90°

Figure 7: Failure modes of different coal-rock combined bodies with different prefabricated fissure angles.

propagates inside the rock mass, as shown in the circle in Figure 7(g). When the inclination angles of the prefabricated cracks are 0°, 15°, and 30°, the failure mode of the CRCB is tensile-shear composite failure. The coal and rock masses in the CRCB are damaged, and the cracks first start propagating near the tip of the prefabricated crack, and then, expanding and penetrating cause the CRCB to reach the peak strength and eventually fail. When the inclination angles of the prefabricated cracks are 45° and 60°, both the coal and rock samples of the CRCB are damaged. Among them, the coal samples are mainly shear failure, and the rock samples are tensile failure with the increase of axial stress. The failure surface and the vertical direction form a certain angle to gradually deflect and finally coincide with the vertical direction. The crack expansion shape in the rock mass is basically S-shaped. The crack propagation and failure process are as follows: under the axial stress, the prefabricated crack of the rock mass slips, a small number of microcracks are generated on both sides of the joint surface, and an upward extending tensile crack is formed on the upper part of the joint surface. At the same time, the microcracks near the two tips of the joint gather and nucleate; when the axial stress increases, they expand upward in the coal sample and the rock sample to form tensile cracks, while the joint surface will continue to slip and expand; when the axial stress continues to increase, the tensile cracks will continue to increase. The extension crack continues to propagate until the total failure of CRCB.

3.4. Acoustic Emission Characteristic Analysis. Coal and rock will release energy in the form of elastic waves (acoustic

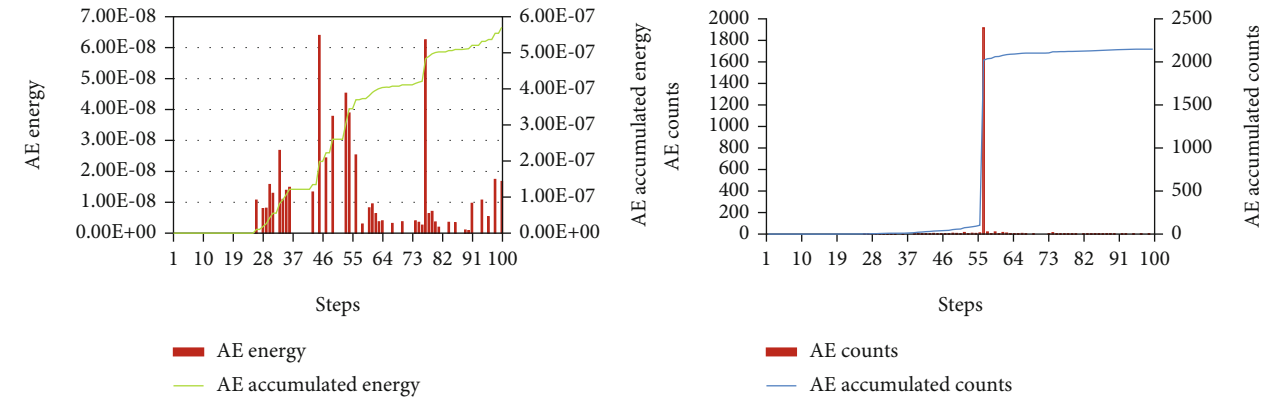

(a) intact

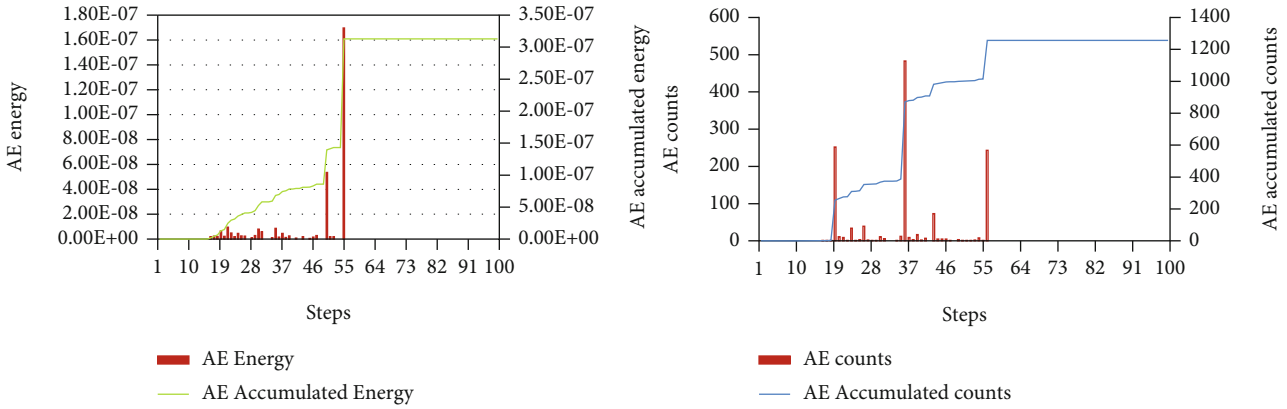

(b) α=0°

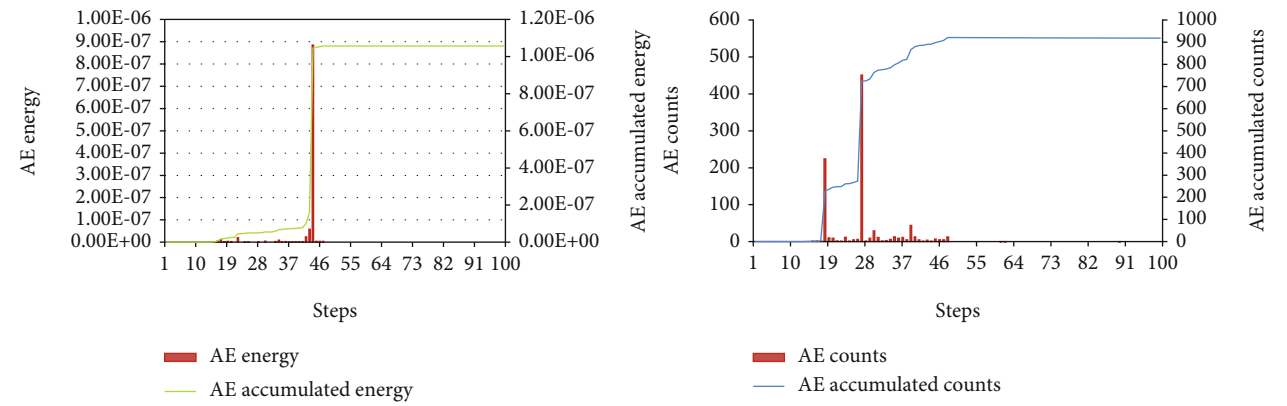

(c) α=15°

Figure 8: Continued.

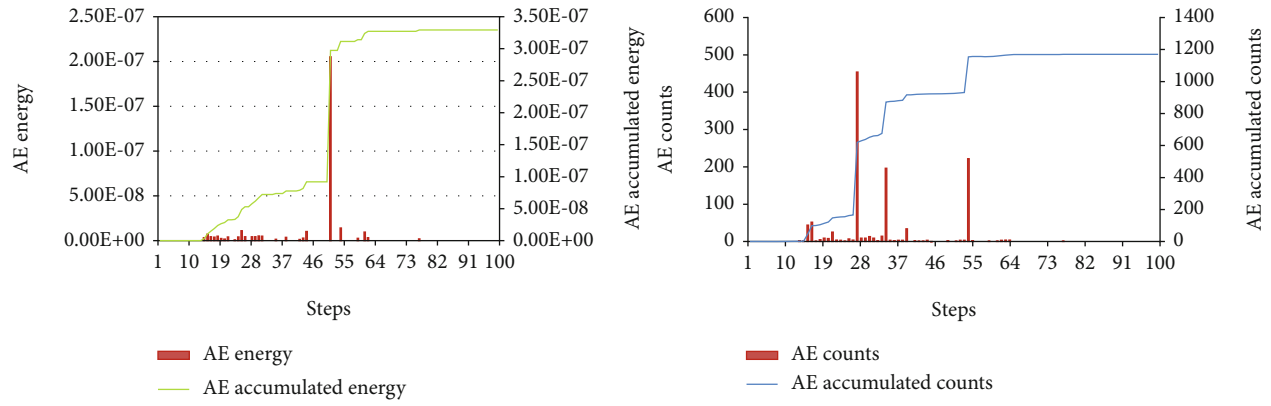

(d) α=30°

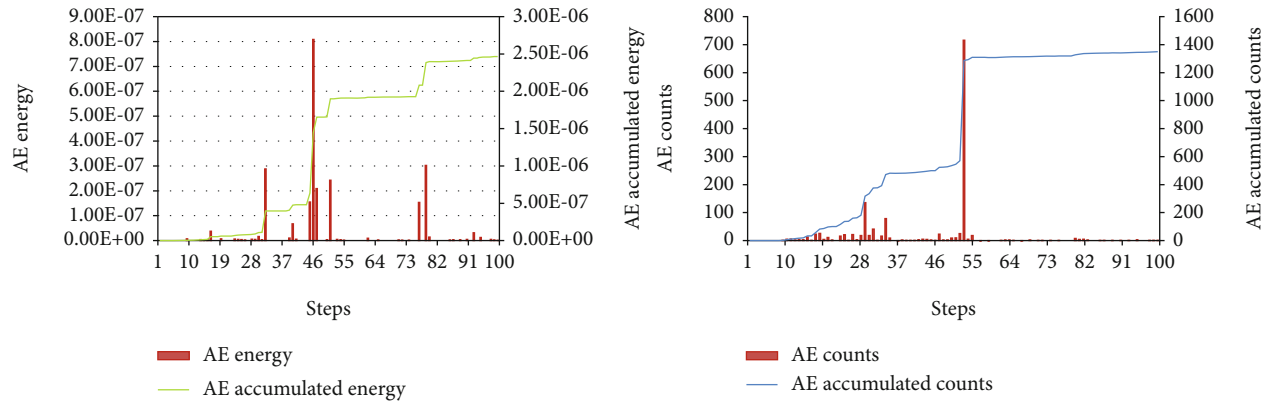

(e) α=45°

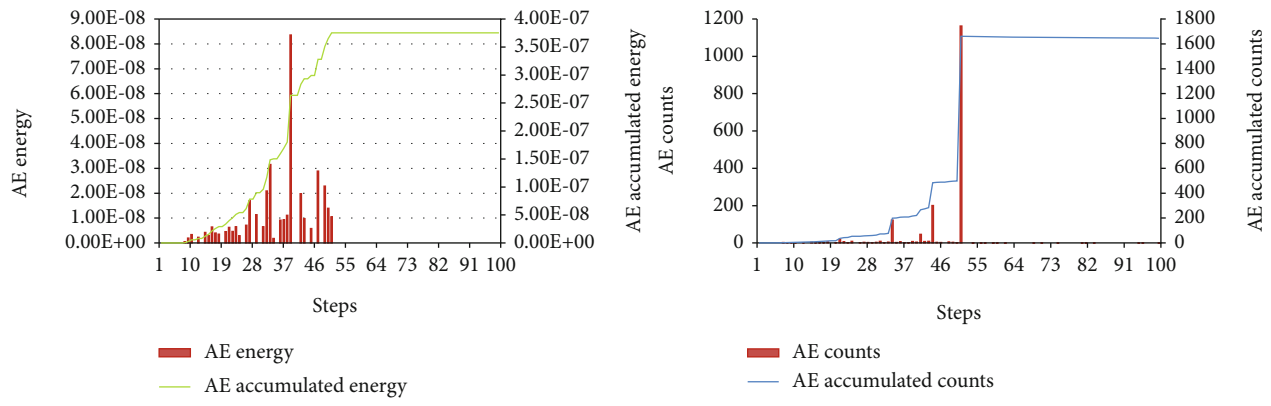

(f) α=60°

Figure 8: Continued.

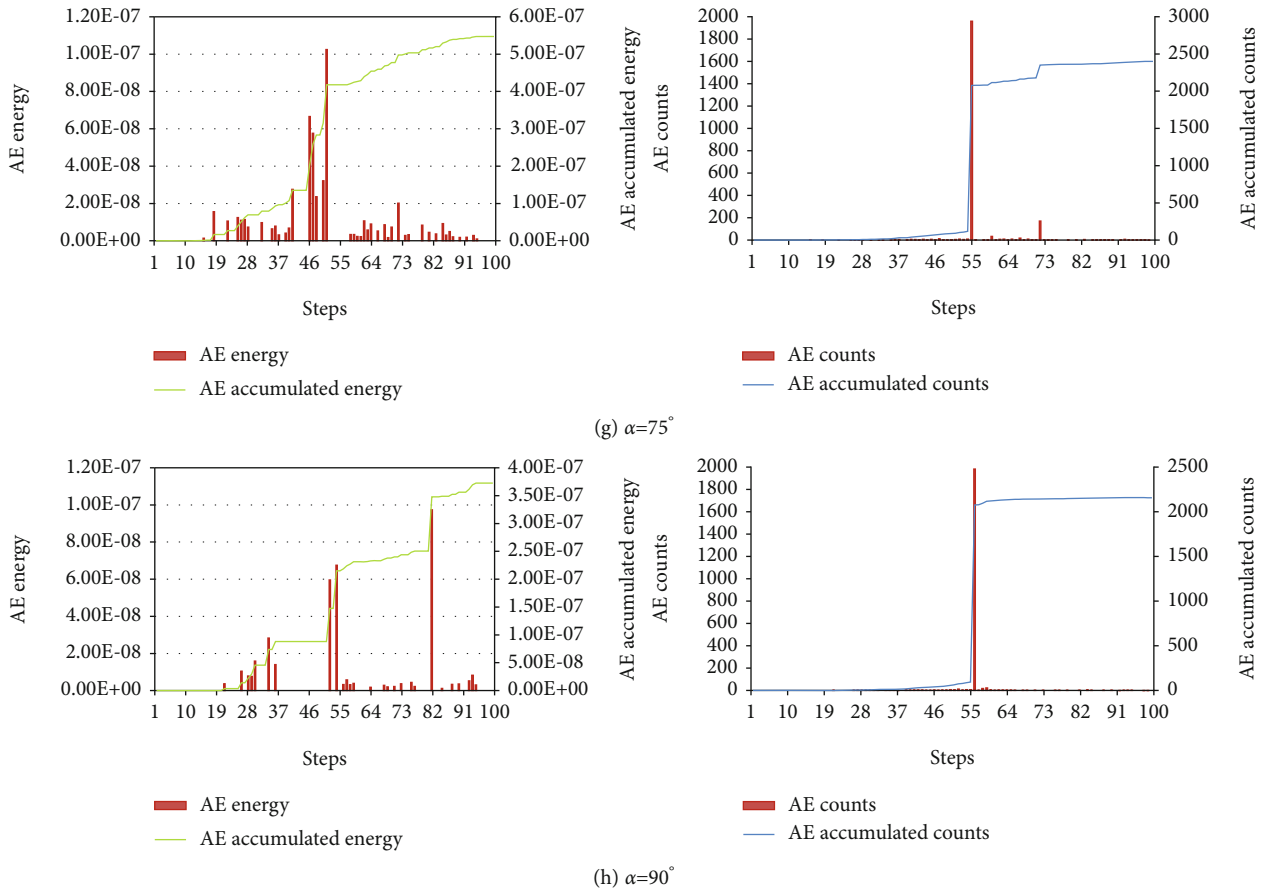

Figure 8: Acoustic emission characteristic curves of coal-rock combined bodies with different prefabricated fissure angles.

emission) during its deformation and failure process [16]. By analyzing acoustic emission parameters, the characteristics of coal and rock deformation and failure can be better understood.

The acoustic emission of the rock in the process of failure and deformation reflects the evolution process of its internal crack initiation, propagation, and penetration failure. It can be seen from Figure 8 that the acoustic emission characteristics of the CRCB with prefabricated fracture of different inclination angles have a general law: At the beginning of loading, no acoustic emission events can be detected because the internal crack is closed; and then, only a small amount of acoustic emission events are generated in the elastic phase. As the load continues to increase to the plastic deformation stage, the internal cracks expand, and more acoustic emission events are generated. Near the peak loading, a large number of acoustic emissions are produced, and the number of acoustic emission events reaches the maximum, which can be used as a precursor to the failure of the CRCB. In the postpeak stage, a certain acoustic emission signal will be generated due to the further propagation and penetration of cracks. At the same time, as shown in Figure 8, the influence of the prefabricated crack inclination angle in CRCB on its acoustic emission characteristics under uniaxial compression can be found: the total number of acoustic emission events as a whole decreases first and then increases with the increase of the prefabricated fracture inclination angle. The CRCB has the highest number of acoustic emission events (2399) when $\alpha = 75^\circ$ (Figure 8(f)), followed by the intact CRCB (2148), which is mainly caused by the development and expansion of the crack tip. The single largest acoustic emission events first decrease and then increase with the increase of the prefabricated fracture inclination angle, and its ratio to the total number of cumulative acoustic emission events is 0.89, 0.38, 0.78, 0.38, 0.53, 0.70, 0.81, and 0.93, respectively, which are consistent with the stress-strain curve in Figure 3 and indicate that intact CRCB and CRCB with prefabricated crack when $\beta = 75^\circ$ and $\beta = 90^\circ$ have strong brittleness, while other CRCB with different prefabricated fracture inclination angles show a certain degree of postpeak plasticity. The single peak acoustic emission events of the CRCB is located after its peak strength when $\alpha = 45^\circ$ (Figure 8(d)) and $\alpha = 60^\circ$ (Figure 8(e)). The number of steps (strain) corresponding to the peak acoustic emission counts of the other CRCB first decreases and then increases with the increase of the inclination angle of the prefabricated fracture, which is consistent with the peak strength of the CRCB. The single peak acoustic emission events and the peak strength correspond to the same strain, indicating that after the peak strength, the CRCB with 45° and 60° prefabricated cracks further expand and penetrate, so it is unreliable to confirm the failure of CRCB by single peak acoustic emission events.

The failure of coal and rock mass under stress is a process of energy absorption and release, and the energy of acoustic

emission reflects the elastic energy released when the cracks inside the coal and rock are generated or expanded [30, 31]. From Figure 8, the accumulative amount of acoustic emission energy increases with the increase of strain. In the initial stage of loading, although the number of acoustic emission events of the CRCB is small, the acoustic emission energy gradually accumulates. When the energy accumulates to a certain extent, the CRCB reaches its peak strength, and the acoustic emission count increases rapidly. It can also be seen from Figure 7 that during the uniaxial compression of different CRCB, the cumulative energy of acoustic emission in descending order is as follows: 45°, 15°, intact CRCB, 75°, 60°, 90°, 30°, and 0°, indicating that the cumulative energy of acoustic emission has a nonlinear relationship with the strength of the CRCB with different inclination angles of prefabricated fracture. The cumulative energy before the peak value of acoustic emission events is as follows: 75°, intact CRCB, 60°, 90°, 45°, 0°, 30°, and 15°, so from the perspective of acoustic emission energy, the outburst proneness of the CRCB with 75° prefabricated fissure is higher than that of the intact CRCB. The single peak acoustic emission energy is located before the peak strength of CRCB for $\alpha = 60°$, $\alpha = 75°$, and intact CRCB, while it is located after the peak strength of CRCB for $\alpha = 0°$, 15°, 30°, 45°, and 90°, which shows the influence of the cracks in the rock mass and their inclination angle on the postpeak characteristics of the CRCB under uniaxial compression.

4. Conclusion

(1) The inclination angle of the cracks in CRCB will affect its crack initiation stress. When the crack inclination angle is around 45°, the crack initiation stress is the smallest, and the numerical simulation results are consistent with the theoretical analysis

(2) The inclination angle of CRCB affects the propagation mode of the crack. The secondary cracks of CRCB with prefabricated fracture of 0°, 15°, and 30° initiated and expanded near the tip of the main crack, and the secondary cracks of 45°, 60°, and 75° initiated and expanded from the tip of the main crack

(3) The inclination angle of CRCB will affect its strength. When $\alpha = 15°$, the peak strength of the CRCB is the lowest. When $\alpha < 15°$, the peak strength of the CRCB decreases with the increase of the crack inclination angle. When $\alpha > 15°$, the peak strength of the CRCB increases with the increase of the inclination angle of the prefabricated fissure

(4) The inclination angle of CRCB will affect its failure modes. The failure of the intact CRCB and the CRCB with 90° and 75° prefabricated fissures mainly occurs in the coal, and it is a double-shear failure mode, and the crack propagation is type Λ. When the inclination angles of the prefabricated cracks are 0°, 15°, and 30°, the failure mode of the CRCB is tensile-shear composite failure. When the inclination angles of the prefabricated cracks are 45° and 60°, the coal samples are mainly shear failure, and the rock samples are tensile failure with the increase of axial stress

(5) The existence of cracks in CRCB will affect its brittleness and plastic characteristics. The acoustic emission results indicate that intact CRCB and CRCB with prefabricated crack when $\alpha = 75°$ and $\alpha = 90°$ have good brittleness, and other CRCB with different prefabricated fracture inclination angles show a certain degree of postpeak plasticity

Data Availability

All data used to support the findings of this study are included within the article, and there are not any restrictions on data access.

Conflicts of Interest

The authors declare no conflicts of interest.

Acknowledgments

This paper was supported by the Natural Science Foundation of the Jiangsu Higher Education Institutions of China (No. 20KJB440002), the National Natural Science Foundation of China (Project Nos. 51804129, 51808246, and 51904112), China Postdoctoral Science Foundation (No. 2020M671301), the Postdoctoral Science Foundation of Jiangsu Province (Nos. 2019K139 and 2019Z107), the Huai'an Science and Technology Plan project (No. HAB201836), the Industry Education Research Cooperation Projects in Jiangsu Province (No. BY2020007), the Undergraduate Innovation and Entrepreneurship Training Program (No. 202011049111XJ), and the Foundation of Huaiyin Institute of Technology (No. Z301B20530).

References

[1] K. Wang and F. Du, "Coal-gas compound dynamic disasters in China: a review," *Process Safety and Environmental Protection*, vol. 133, pp. 1–17, 2020.

[2] L. Yang, F. Gao, X. Wang, and J. Li, "Energy evolution law and failure mechanism of coal-rock combined specimen," *Journal of China Coal Society*, vol. 44, no. 12, pp. 3894–3902, 2019.

[3] J. Zuo, H. Xie, A. Wu, and J. Liu, "Investigation on failure mechanism and mechanical behaviors of deep coal-rock single body and combined body," *Chinese Journal of Rock Mechanics and Engineering*, vol. 30, no. 1, pp. 84–92, 2011.

[4] F. du, K. Wang, X. Zhang, C. Xin, L. Shu, and G. Wang, "Experimental study of coal-gas outburst: Insights from coal-rock structure, gas pressure and adsorptivity," *Natural Resources Research*, vol. 29, no. 4, pp. 2481–2493, 2020.

[5] J. Zuo, J. Wang, and Y. Jiang, "Macro/meso failure behavior of surrounding rock in deep roadway and its control technology," *International Journal of Coal science & Technology*, vol. 6, no. 3, pp. 301–319, 2019.

[6] F. Gong, H. Ye, and Y. Luo, "Rate effect on the burst tendency of coal-rock combined body under low loading rate range," *Journal of China Coal Society*, vol. 42, no. 11, pp. 2852–2860, 2017.

[7] F. Gong, H. Ye, and Y. Luo, "The effect of high loading rate on the behaviour and mechanical properties of coal-rock combined body," *Shock and Vibration*, vol. 2018, Article ID 4374530, 9 pages, 2018.

[8] J. Zuo, Y. Chen, H. Song, and X. Wei, "Evolution of pre-peak axial crack strain and nonlinear model for coal-rock combined body," *Chinese Journal of Geotechnical Engineering*, vol. 39, no. 9, pp. 1609–1615, 2017.

[9] Y. Chen, J. Zuo, D. Liu, Y. Li, and Z. Wang, "Experimental and numerical study of coal-rock bimaterial composite bodies under triaxial compression," *International Journal of Coal Science & Technology*, 2021.

[10] J. Cao, Q. Dai, Y. Zhou, and D. Ma, "Failure mechanism and strength of coal-rock combination bodies considering dip angles and fractal characteristics of interface," *Journal of Central South University (Science and Technology)*, vol. 49, no. 1, pp. 175–182, 2018.

[11] X. Liu, Y. Tan, J. Ning, Y. Lu, and Q. Gu, "Mechanical properties and damage constitutive model of coal in coal-rock combined body," *International Journal of Rock Mechanics and Mining Sciences*, vol. 110, pp. 140–150, 2018.

[12] Z. Xie, N. Zhang, F. Meng, C. Han, Y. An, and R. Zhu, "Deformation field evolution and failure mechanisms of coal-rock combination based on the digital speckle correlation method," *Energies*, vol. 12, no. 13, pp. 1–14, 2019.

[13] F. Du and K. Wang, "Unstable failure of gas-bearing coal-rock combination bodies: Insights from physical experiments and numerical simulations," *Process Safety and Environmental Protection*, vol. 129, pp. 264–279, 2019.

[14] Y. Chen, J. Zuo, H. Song, L. Feng, and G. Shao, "Deformation and crack evolution of coal-rock combined body under cyclic loading-unloading effects," *Journal of Mining & Safety Engineering*, vol. 35, no. 4, pp. 826–833, 2018.

[15] Z. Zhao, W. Wang, L. Wang, and C. Dai, "Compression-shear strength criterion of coal-rock combination model considering interface effect," *Tunnelling and Underground Space Technology*, vol. 47, no. 3, pp. 193–199, 2015.

[16] S. Dong, A. Li, Y. Ji, Y.-x. Yang, and Q. Mu, "Mechanical and failure characteristics of rock-coal-rock combined body under different strain rates: a numerical study from micro perspective," *Geotechnical and Geological Engineering*, vol. 39, no. 1, pp. 185–191, 2021.

[17] C. Li, Y. Xu, Y. Zhang, and H. Li, "Study on energy evolution and fractal characteristics of cracked coal-rock-like combined body under impact loading," *Chinese Journal of Rock Mechanics and Engineering*, vol. 38, no. 11, pp. 2231–2241, 2019.

[18] D. Yin, S. Chen, B. Chen, X. Liu, and H. Ma, "Strength and failure characteristics of the rock-coal combined body with single joint in coal," *Geomechanics and Engineering*, vol. 15, no. 5, pp. 1113–1124, 2018.

[19] D. Yin, S. Chen, B. Chen, L. Jiang, T. Meng, and W. Wang, "Simulation study on effects of coal persistent joint on strength and failure characteristics of rock-coal combined body," *Journal of Mining & Safety Engineering*, vol. 35, no. 5, pp. 1054–1062, 2018.

[20] W. F. Brace and E. G. Bombolakis, "A note on brittle crack growth in compression," *Journal of Geophysical Research*, vol. 68, no. 12, pp. 3709–3713, 1963.

[21] H. Horii and S. Nemat-Nasser, "Compression-induced microcrack growth in brittle solids: axial splitting and shear failure," *Journal of Geophysical Research*, vol. 90, no. B4, pp. 3105–3125, 1985.

[22] X. Zhou and Y. Zhang, *Constitutive Theory of Stress Relief Rock Mass and Its Application*, Science Press, Beijing, 2007.

[23] P. Lin, K. Huang, R. Wang, and W. Zhou, "Crack growth mechanism and failure behavior of specimen containing single flaw with different angles," *Chinese Journal of Rock Mechanics and Engineering*, vol. 24, pp. 5652–5658, 2005.

[24] E. Lajtai, "Strength of discontinuous rocks in direct shear," *Geotechnique*, vol. 19, no. 2, pp. 218–233, 1969.

[25] Huiwang, *Numerical simulation of fractured rock failure process and related laws, [Dissertation]*, Anhui University of Science&Technology, 2015.

[26] C. Tang, S. Wang, and F. Yufang, *Numerical Experiment of Rock Failure Process*, Science Press, Beijing, 2012.

[27] Z. Liang, C. Tang, H. Li, T. Xu, and T. Yang, "A numerical study on failure process of transversely isotropic rock subjected to uniaxial compression," *Roak and Soil Mechanics*, vol. 26, no. 1, pp. 57–63, 2005.

[28] L. Cunbao, H. Xie, and L. Xie, "Experimental and theoretical study on the shale crack initiation stress and crack damage stress," *Journal of China Coal Society*, vol. 42, no. 4, pp. 969–976, 2017.

[29] M. Gao, T. Li, L. Meng et al., "The method to identify characteristic stresses of rock in different stages during failure process," *Chinese Journal of Rock Mechanics and Engineering*, vol. 35, no. S2, pp. 3577–3588, 2016.

[30] D. Zhang, C. Liu, Y. Zhou, and D. Ma, "Characteristics of fracture mechanism and acoustic emission of rock-coal combined body with prefabricated fissure," *Geotechnical and Geological Engineering*, vol. 38, pp. 6245–6254, 2020.

[31] F. du, K. Wang, G. Wang, Y. Jiang, C. Xin, and X. Zhang, "Investigation of the acoustic emission characteristics during deformation and failure of gas-bearing coal-rock combined bodies," *Journal of Loss Prevention in the Process Industries*, vol. 55, pp. 253–266, 2018.